CCFE
CULHAM CENTRE FOR FUSION ENERGY

UK Atomic Energy Authority

UKAEA-CCFE-PR(23)85

J.W. Berkery, G. Xia, J.M. Bialek, S.A. Sabbagh, Z.R. Wang, C. Ham, A. Thornton, Y.Q. Liu

Projected Global Stability of High Beta MAST-U Spherical Tokamak Plasmas

Projected Global Stability of High Beta MAST-U Spherical Tokamak Plasmas

J.W. Berkery, G. Xia, J.M. Bialek, S.A. Sabbagh, Z.R. Wang, C. Ham, A. Thornton, Y.Q. Liu

This is a preprint of a paper submitted for publication in Plasma Physics and Controlled Fusion

Projected Global Stability of High Beta MAST-U Spherical Tokamak Plasmas

J W Berkery[1], G Xia[2], S A Sabbagh[1], J M Bialek[1], Z R Wang[3], C J Ham[2], A Thornton[2] and Y Q Liu[4]

[1] Department of Applied Physics and Applied Mathematics, Columbia University, New York, New York 10027, USA
[2] Culham Centre for Fusion Energy, UKAEA, Abingdon, OX14 3DB, UK
[3] Princeton Plasma Physics Laboratory, Princeton, New Jersey, 08543, USA
[4] General Atomics, P.O. Box 85608, San Diego, California 92186-5608, USA

E-mail: jberkery@pppl.gov

Received xxxxxx
Accepted for publication xxxxxx
Published xxxxxx

Abstract

Assessment of the limits of stability of tokamak plasmas is key to operation in high fusion performance ranges without disruption of the plasma current. Projected equilibria have been generated for the MAST-U spherical tokamak experiment, an upgrade of the previous MAST device, in order to prepare for operation. These equilibria are scanned in pressure and current profiles, and assessed with the DCON and MARS-F stability codes to find the so-called "no-wall" beta limit, above which resistive wall mode instabilities can be expected in the absence of other stabilising effects. The no-wall limit was generally found to increase as plasma internal inductance increased. The equilibria are also assessed for the "with-wall" limit, theoretically the highest achievable performance point, again with the DCON and MARS-F codes, including different approximate axisymmetric walls, and with the VALEN code which includes a 3D model of the surrounding conducting structure. Similar limits were found, despite the difference between the 2D and 3D codes in the treatment of the wall. Conducting passive stabilisation plates, which were newly installed in MAST-U, are in a region of significant mode perturbation when the plasma β_N is sufficiently high and eddy currents are driven in these structures. Due to the increased stabilising effect of the wall in MAST-U vs. MAST, a significant gap exists between the approximate no-wall limits of β_N/l_i = 6.44 and 7.13, found from DCON and MARS-F respectively, and the with-wall limits of β_N/l_i = 8.01 and 8.53 for the equilibrium profiles analysed in this study. This opens a region of high beta operating space in MAST-U for potentially stable operation if non-ideal effects or active control can stabilise the resistive wall mode.

Keywords: disruptions, stability, spherical tokamak

(Some figures may appear in colour only in the online journal)

1. Introduction

High pressure plasmas in fusion devices are subject to modes of instability that are global, not localized to a small portion of the plasma volume like the edge or a magnetic island. These global modes can grow and lead to disruption of the plasma current and contact between the plasma and the walls of the device. In future devices these disruptions could potentially damage the device due to high electromagnetic forces on the vessel or heat loads on the plasma facing components. These modes also can be stabilised, either passively by processes within the plasma itself, or actively by application of specific magnetic fields or heating actuators. Proper assessment of the limits of stability in plasmas is key to operation in high fusion

performance ranges. The MAST-U spherical tokamak experiment, an upgrade of the previous MAST device [1], can uniquely leverage the low aspect ratio, high elongation, high beta, flexible heating, and 3D coil capabilities of the device to test stability calculations and modelling that support disruption prediction and avoidance. Although disruptions in MAST-U may be tolerable from an engineering perspective, understanding them is important for future devices where they may not be. Two of the main objectives of the MAST-U research plan are (i) Adding to the knowledge base for ITER: for which disruption prediction and avoidance are both timely and paramount, and (ii) Exploring the case for a future fusion device based on the spherical tokamak (ST): which must reliably operate a plasma at high performance, free of significant transient events that would terminate the plasma or significantly change its fusion neutron output. MAST-U also aims to study the stability of plasmas at new low plasma collisionality values in the ST, as this parameter has been identified to be important for improved stability in high beta plasmas [2]. Understanding of stability and disruption prediction and avoidance is a critical companion to the energy confinement studies planned on MAST-U.

If a plasma displacement from an equilibrium state causes the potential energy in the plasma and the surrounding vacuum to decrease and the displacement to grow, then it is considered an unstable mode of the plasma. By considering a series of plasma equilibria with increasing pressure and no effects of the plasma conducting structure, the point can be found where the change in potential energy, δW, crosses from positive to negative, indicating the so-called no-wall limit. Theoretically, above this limit the ideal kink-ballooning mode will grow on an Alfven time scale (typically the fastest to consider in this system (~ 100 μs). The effect of the wall is to slow the growth to the significantly lower time scale of the penetration of the magnetic flux through the conducting structure (~ 10 ms), allowing a new branch of the kink mode called the resistive wall mode (RWM) [3]. At high enough pressure, even an ideally conducting wall cannot prevent the growth of the ideal kink, leading to the so-called "with-wall" limit. Even this stability analysis is incomplete, however, as there are kinetic effects of particle motions that act to stabilise plasmas above the no-wall limit. Still, assessment of the ideal stability limits is important as a basis for kinetic stability analysis and for understanding other processes such as resonant field amplification, which happen in the proximity of the no-wall limit. Even if plasmas remain stable as the no-wall limit is crossed, other unintended consequences can occur, such as error field amplification and rotation braking [4]. Additionally, this stability assessment can be used by a code such as DECAF [5,6] which uses various stability modules, including an ideal stability assessment assisted by machine learning techniques [7], to monitor and forecast the potential for plasma disruption.

The ideal stability of plasmas in MAST, the predecessor to MAST-U, has been previously studied [8,9,10]. In separate studies, the no-wall normalized beta limit was found to be in the 4-5 range with the with-wall limit in the 5-6 range [10], or a higher no-wall limit >5 with a smaller wall stabilisation gap [8]. The expectation is that MAST-U will have similar stability properties, but the no-wall limits may differ if MAST-U is operated in different regimes, and the with-wall limit may differ due to changes in the conducting structure during the upgrade.

In the present study we use the DCON, MARS-F, and VALEN codes to assess the stability of MAST-U plasmas. The DCON [11] and MARS-F [12] stability codes have long been used to calculate the change in potential energy, δW, in a plasma, while VALEN [13] can assess the impact of three dimensional conducting structures. First, in section 2, the projected MAST-U equilibria that we are studying are described. In section 3, the assessment of the no-wall limit is discussed. In section 4 two methods, using an axisymmetric wall and a 3D wall, are used to determine the effect of the wall on stability. Finally, conclusions of the study are drawn.

2. Projected MAST-U equilibria

In order to prepare for operation of the MAST-U device, projected plasma equilibria were generated. The equilibria are generated with a set of coil current and plasma current profiles which are then iterated to equilibrium using the FIESTA code [14]. The current profiles are derived from TRANSP [15] modelling, and constraints on the boundary location were also provided in order to get the magnetic field in terms of the coil currents.

Four different projected equilibria are presently considered. The last closed flux surfaces of these are shown in Fig. 1, along with the locations of various conducting structures and the axisymmetric wall used by the MARS-F code later in section IV-A. Shown in red is the "conventional" case, which has an internal inductance, $l_i = \langle B_p^2 \rangle / \langle B_p \rangle^2$ (B_p is the poloidal magnetic field and $\langle \ldots \rangle$ represents volume average), of about 0.6, pressure peaking factor $F_p = p_0/\langle p \rangle = 2$, and aspect ratio, $A = 1.72$. In green, the "SuperX" equilibrium, which is quite similar to the conventional case, is intended as a target for MAST-U experiments exploring the super X divertor concept [16]. In black and blue, respectively, are the "k25" and "low elongation" equilibria, which are both at a lower aspect ratio of 1.55, with higher and lower elongation than the conventional case, as can be seen in the figure. In each case the plasma current is ~1MA, except the low elongation case, which is at ~1.2MA and additionally has a non-monotonic safety factor, q, profile.

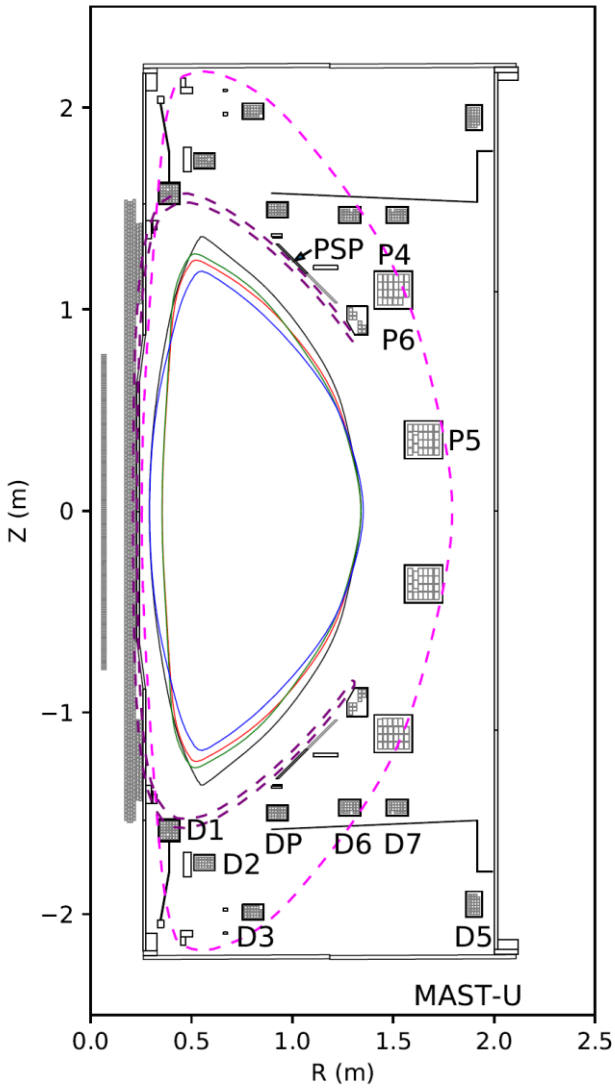

Figure 1. Last closed flux surfaces of four MAST-U equilibria: k25 (black), Conventional (red), Low Elongation (blue), and SuperX (green). The dashed magenta line shows the axisymmetric equivalent superconducting wall used by the MARS-F code, while the dashed purple line shows the wall with a poloidal gap on the large major radius side used by the DCON code. Only toroidally continuous conducting structures, including the "P" and "D" poloidal field coil cases, are shown (no carbon tiles). Additionally, the outer half of the passive stabilisation plates (PSP) are shown, although they have toroidal gaps.

In order to make use of these equilibria for stability studies, it was necessary to increase the pressure until unstable mode levels were found. This was achieved with the CHEASE code [17], with which it is easy to self-similarly scale the pressure profile while keeping total plasma current constant. In this way, β_N is scanned, while other relevant parameters for ideal stability, such as pressure peaking and aspect ratio are also constant. The q profile, and therefore l_i, change during the scan, but only slightly, as indicated in the example scan in Fig. 2 for the k25 equilibrium. The implicit assumption is that increased power from neutral beam injection would be used to increase the pressure experimentally in MAST-U. Not all the scenarios explored here would be experimentally realizable on MAST-U during its initial operation with 5 MW of beam power, however plans exist for an upgrade to 10 MW after a few years of operation [1].

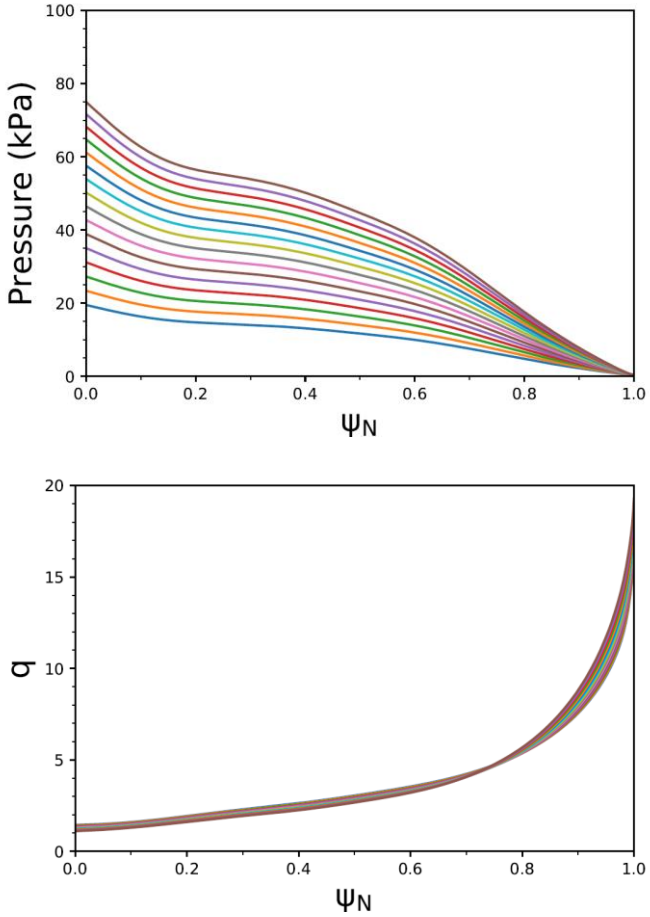

Figure 2. Pressure and q profiles vs. normalized magnetic flux for the pressure scan of the k25 MAST-U equilibrium.

3. No-wall beta limit calculations

One recent approach to assessing ideal stability was to use the DCON code on a database of more than 5,000 equilibria from the NSTX spherical tokamak [18]. This work has generated a parametrized forecasting model for $\beta_N^{no\text{-}wall}$ with variables including aspect ratio A, pressure peaking F_p, and internal inductance l_i. This model has been implemented in the DECAF code and tested for NSTX and NSTX-U discharges. Additionally, machine learning techniques such as neural networks and random forests are now being used to refine and supplement the ideal stability model [7].

Ideal stability analysis for MAST-U plasmas, using kinetic equilibrium reconstructions, will provide a critical validation test of the applicability of the initial ideal stability forecasting

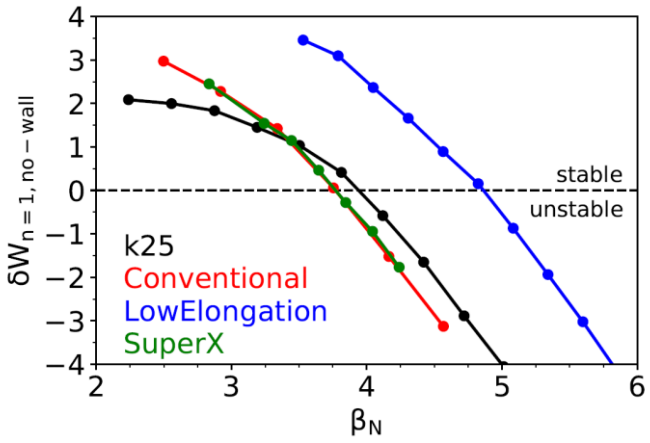

Figure 3. DCON-calculated δW vs. β_N for a collection of projected MAST-U equilibria.

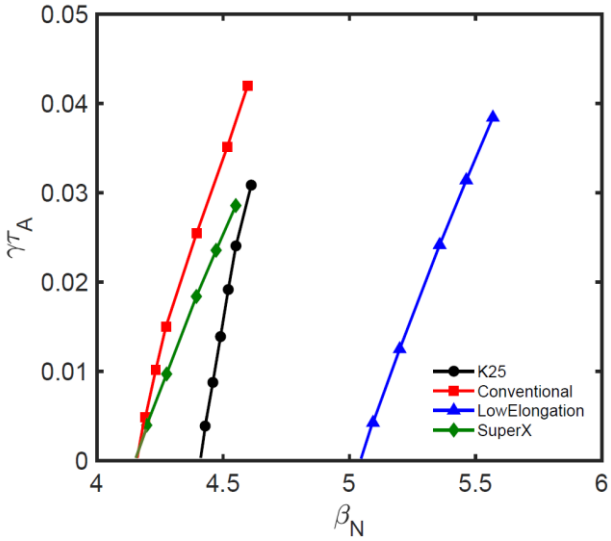

Figure 4. MARS-F calculated ideal growth rates with no wall for the projected MAST-U equilibria using the same colors as Fig. 3.

model in DECAF, especially the dependence on A, l_i, and F_p, leveraging the low A and l_i operating regime produced in MAST-U plasmas. Understanding the physical reasons for any differences that are found from the analysis, and implementation of such differences will significantly enhance the extrapolability of the revised ideal stability forecasting model for general applicability for all tokamaks.

Plans also exist for experimentally probing the ideal MHD no-wall limit in MAST-U using active MHD spectroscopy, a technique by which the resonant field amplification (RFA) of a low frequency applied n = 1 field is measured. Increasing RFA amplitude is correlated with decreasing mode stability [19]. Low frequency MHD spectroscopy has been performed on MAST [9,10] and compared to ideal stability calculations [10,7], and this past analysis gives confidence that the technique can be used more extensively to diagnose plasma stability in MAST-U.

3.1 Pressure scan using CHEASE

The collection of projected equilibria for MAST-U provide a platform for testing the ideal stability of plasmas in the new device. Each equilibrium described in the previous section was scaled with the CHEASE code in pressure, holding the plasma current constant, which provides a scan in normalized beta. These equilibrium scans were assessed with the DCON code with the no wall boundary condition, and the results are shown in Fig. 3. One can see that the no-wall limit ranges from β_N of 3.77 to 4.88 for these cases. Additionally, the same pressure scans were analysed with the MARS-F code, which calculated growth rate normalized by the Alfven time, $\gamma\tau_A$, the no-wall limit being the beta at which the growth rate becomes positive. Figure 4 shows the MARS-F calculations for the four projected equilibria. In each case, the MARS-F values are somewhat larger (within about 10%) than the DCON values, ranging from 4.14 to 5.05.

Subsequently, the various beta scans can be used to create a plot of the stability space in various parameter spaces. For example, in Fig. 5 the calculated points of crossing the no-wall limits in both DCON and MARS-F are plotted on a diagram of β_N vs l_i, the internal inductance. Also included in the plot are the calculations of the with-wall limits, which will be explained in the next section. Approximate demarcations of the no-wall limit of β_N/l_i = 6.44, in the dashed grey line from DCON, and β_N/l_i = 7.13, in the solid grey line from MARS-F, are found simply by fitting the four stable-to-unstable transition points to a line with no intercept. The DCON computed n = 1 no-wall limit is quite similar to one found for the NSTX device [18]. It is worth noting that studies in MAST that mostly found higher no-wall limits than these levels for MAST-U were typically performed for plasmas with higher internal inductances, in the range of unity and above [8,10].

From Fig. 5 it is apparent that this simple β_N/l_i formulation does not capture all of the nuances of the no-wall limit. For example, the blue low elongation case has a higher stability limit than the black k25 case at a similar internal inductance. With only four equilibria analysed, it is difficult to determine the reason for the difference in stability between these cases. It is worth noting that these cases both have a lower aspect ratio of about 1.55 than the conventional and SuperX, which are at $A \sim 1.72$. A general decline of the no-wall beta limit with increasing aspect ratio is consistent with prior expectation [18] but again doesn't explain the difference between the k25 and low elongation cases. Naturally, the elongation itself is a factor in the stability, but the lowest elongation case having

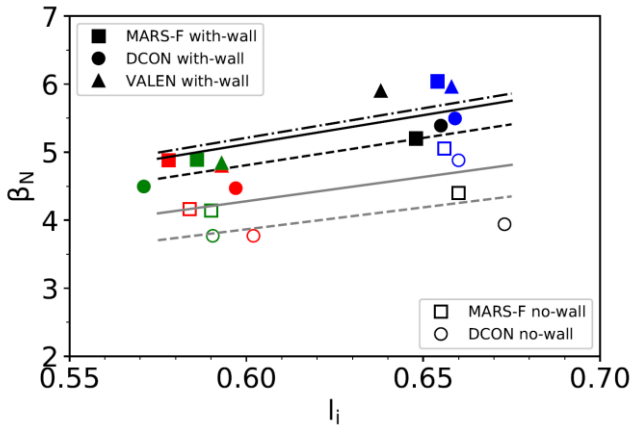

Figure 5. Stability map in the parameter space of β_N vs. l_i, for a collection of projected MAST-U equilibria using the same colors as Fig. 3. Square markers and solid lines are from MARS-F, circle markers and dashed lines are from DCON, and triangle markers and dash-dot lines are from VALEN. Open markers and grey lines are for the no-wall limit and solid markers and black lines for the with-wall limit.

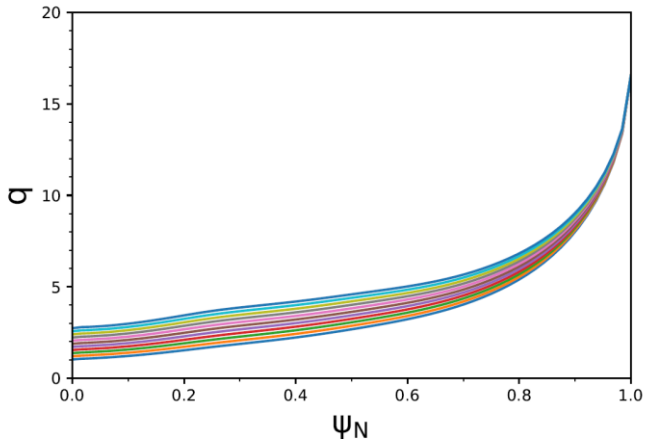

Figure 6. q profile scan vs. normalized magnetic flux for the 2D CORSICA profile scan of the k25 MAST-U equilibrium, scanning q_0.

the highest stability runs counter to expectation. Additionally, although there is some evidence of increased triangularity increasing the no-wall limit [20], it doesn't appear to be the case here, as the k25 and low elongation cases have δ below 0.5, while conventional and SuperX have δ above 0.61. The low pressure peaking, $F_p \sim 1.65$, of the low elongation case could possibly be responsible for its greater stability vs. the higher pressure peaking, $F_p \sim 2.2$, in the k25 case. Although a beta limit decrease with pressure peaking factor is not unexpected at higher peaking factors, this is opposite to the trend found in NSTX in a similar, low pressure peaking factor range [18,7]. Finally, it should be noted again that, unlike the other equilibria, the low elongation case has a non-monotonic q profile, with a q_0 of about 2.8, but a q_{min} of about 2.0. This may contribute to the stability in a way that is not easily captured by the global quantities.

3.2 Pressure and q-profile scans using CORSICA

In addition to the pressure scans performed while holding the safety factor profile nearly constant with CHEASE in the previous section, we have also now utilized the CORSICA code [21] to scan both the pressure and q profiles at the same time, thus providing two dimensional parameter scans. While pressure scans essentially the same as demonstrated in Fig. 2a were performed, a q profile scan was performed by changing q_0. This is shown in Fig. 6 for the k25 equilibrium as an example. Effectively, along with the pressure scan which once again provides a scan of β_N, this scan of the q profile provides a scan of l_i. It should be noted again, that not all of these pressure and q profile combinations will be physically realizable in the MAST-U device, but they serve to theoretically explore the parameter space.

The DCON calculations performed in these two dimensional parameter spaces are shown in Fig. 7, for the conventional, k25, and SuperX equilibria (the low elongation equilibria proved difficult to scan the q profile in CORSICA because of the reversed shear).

Figure 7 shows the ideal stability space of β_N vs. l_i, from the two dimensional scans. The coloured contour regions on each plot in Fig. 7 represent an underlying grid of approximately equally spaced 11 by 11 calculation points (a total of 121 calculations with DCON each, minus some points where the calculation failed). In each case, and in agreement with the overall trend in Fig. 5, the no-wall limit increases with l_i in this somewhat narrow range. The values of the no-wall limit are slightly lower than were obtained from the CHEASE generated scans, perhaps due to some particularity of the CORSICA equilibria. However, the levels in the vicinity of just below 4 are consistent with the previous analysis.

4. With-wall stability calculations

The growth of the ideally unstable mode that exists at plasma betas above the no-wall stability limit is slowed from the relatively short Alfven time scale (~ 100 μs) to a longer wall time (~ 10 ms) by the presence of close fitting conducting structure around the plasma. However, if the beta continues to increase there exists another limit where even an ideal conducting wall would no longer prevent the growth of the ideal mode. At this point, the mode is typically named an "internal kink mode". This with-wall limit can be calculated much in the same way as the no-wall limit, but with the addition of a conducting wall in the vacuum region, which modifies the δW.

4.1 Axisymmetric wall using MARS-F

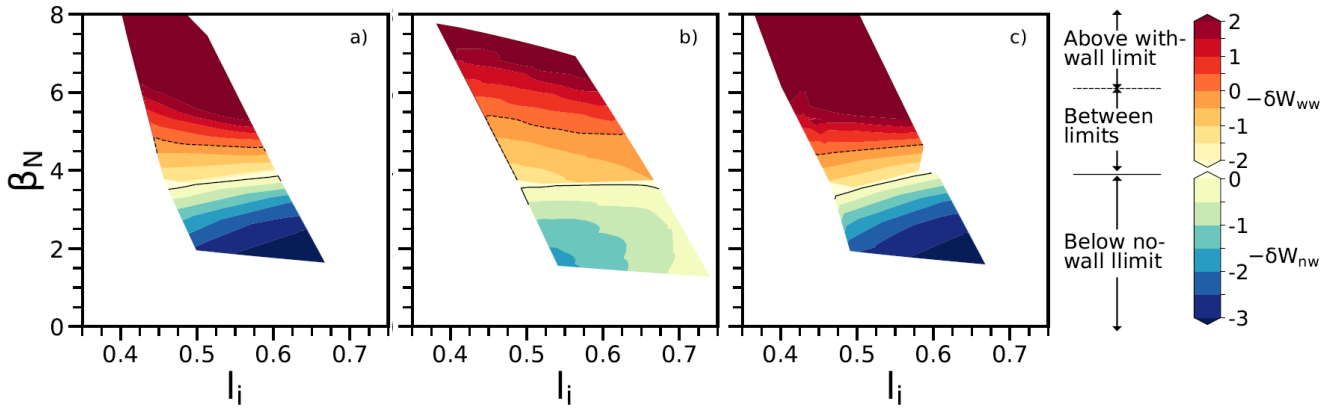

Figure 7. Contours of $-\delta W$ calculated by DCON, in the parameter space of β_N vs. l_i, where contours of $\delta W^{no\text{-}wall}$ are plotted below the no-wall limit (solid line), and $\delta W^{with\text{-}wall}$ above the no-wall limit, for the a) conventional, b) k25, and c) SuperX equilibria. The with-wall limit is indicated by a dashed line.

MARS-F can include a thin, axisymmetric conducting wall for this purpose. For MAST-U the conducting structures are, of course, more complex than a single surface, but their collective effects can be approximated by the wall shown in Fig. 1. When these calculations are performed, the with-wall beta limits are found to be 4.88, 4.89, 5.20, and 6.04 respectively, for the conventional, SuperX, k25, and low elongation equilibria. These points were also plotted on Fig. 5 as solid squares, and the approximate with-wall limit from MARS-F of β_N/l_i = 8.53 was indicated by the solid black line.

4.2 Wall with poloidal gap using DCON

The DCON code is capable of incorporating walls of various geometry, including the one that will be tested here – a C-shaped axisymmetric wall, with a large toroidal gap on the outboard midplane [22]. Figure 1 shows the implementation of this wall type for MAST-U, which is meant to emulate the effects of the conducting material close to the plasma at the top and bottom, including most importantly the passive stabilisation plates. The with-wall beta limits are found to be 4.47, 4.50, 5.39, and 5.50 respectively, for the conventional, SuperX, k25, and low elongation equilibria. These points were also plotted on Fig. 5 as solid squares, and the approximate with-wall limit from DCON of β_N/l_i = 8.01was indicated by the dashed black line. Once again, as with the no-wall limit, the DCON values lie below the MARS-F values, and with a consistent decrement.

DCON was also used for the two-dimensional scan of β_N and l_i with Corsica, as was done without a wall in section 3.2. Contours of $\delta W^{with\text{-}wall}$ are included on Fig. 7 for the parameter space above the no-wall limit. Each with-wall limit is near the value given in the previous paragraph for the actual projected equilibrium, and the trends for each equilibrium is to be fairly constant as l_i is changed in a small range (one slightly decreasing, one slightly increasing).

4.2 Three dimensional conducting structure using VALEN

VALEN is a computer code that uses a mesh circuit formulation for conducting structures surrounding plasmas [13]. VALEN includes the correct resistivities for various materials that comprise the elements of the conducting structure model. A similar capability exists within the LRDFIT codes, and has been used to model plasma startup, including in MAST-U [23]. Here, however, we use VALEN's plasma response model to analyse resistive wall mode (RWM) behaviour. Once DCON calculations of unstable modes are achieved, VALEN analysis can be performed, using the DCON calculation of the *B*-normal distribution on the plasma surface from a series of equilibria over a range of beta values to determine the expected growth rates of resistive wall modes interacting with the conducting structure of the device (as in for the NSTX device, for example, in Ref. [24]). Additionally, VALEN is capable of assessing active feedback control stabilisation of the RWM, although that is beyond the scope of the present study.

It is useful here to make a comparison between the MAST and MAST-U devices, as the conducting structure was changed significantly during the device upgrade. Figure 8 shows the VALEN model of the conducting structures of MAST-U, along with eddy current patterns that will be explained later. The model contains non-axisymmteric 3D ports on the vessel on an otherwise axisymmetric representation of the vacuum vessel, center column, and poloidal field coil cases. Additionally, new stainless steel passive stabilisation plates in the baffle structure in the divertor region that were not present in MAST are included [25]. This structure in particular is

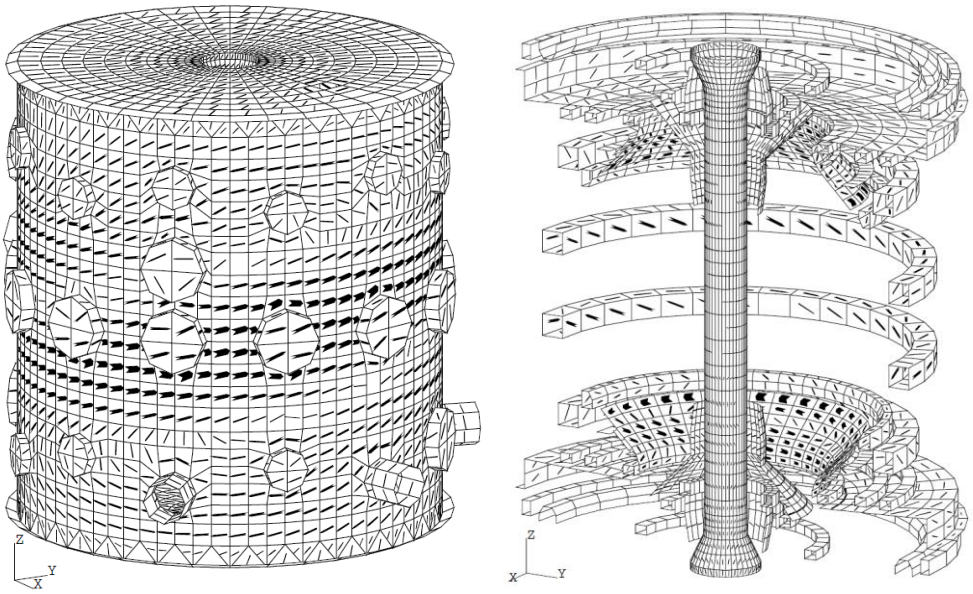

Figure 8. Exterior view and interior detail of the 3D VALEN model of the MAST-U conducting structure. Arrows indicate eddy currents calculated for an $n = 1$ unstable resistive wall mode in the MAST-U projected equilibrium k25, and their thickness is proportional to the current in a given element.

somewhat complex, consisting of 24 plates toroidally that are connected on their bottom halves, with gaps between the upper halves. At the moment in the VALEN model the gaps are not included, so the structure is toroidally continuous. This can potentially be improved in future studies, though, due to VALEN's 3D capability. This new structure close to the plasma surface has implications for the global stability, as we shall see, but also for vertical stability in the device [14].

In a previous VALEN analysis of the MAST device with an unstable mode, the perturbation was concentrated on the outboard midplane, where MAST had little to offer for stabilisation in terms of nearby conducting structure. It is not surprising, then, that when the growth rate was calculated by VALEN in a scan of a dimensionless stability parameter (the ratio of the DCON δW for the plasma to the energy that would have been required to produce the resulting magnetic field distribution without the plasma), the transition between the resistive and ideal branches of the mode (the with-wall limit) occurred at a lower value than, for example, the usual experience for NSTX, which had an array of copper plates for kink mode stabilisation. This indicates that the MAST wall was not able to provide much stabilisation. For discharge 7090 at 0.280 s in MAST, the no-wall limit was predicted to be at about β_N of 5.04 (this discharge was one of a class of very high beta MAST discharges [26]). The with-wall limit, meanwhile, was barely above the no-wall limit, at 5.16. Both of these values are somewhat less than was previously found for the same MAST discharge, using kinetic equilibrium reconstructions [8], and the no-wall limit is somewhat greater than found with a machine learning DCON emulation [7]. However, the point remains that the gap between the two limits was very small – essentially insignificant from an operational standpoint. It is worth stating that, additionally, in Ref. [8] it was noted that the with-wall limit was only 10% above the no-wall limit for multiple discharges, and that "more significant gains in the MAST beta limit could be established if the poloidal field coils were placed closer to the plasma".

In contrast, in present VALEN studies of MAST, we have found that in reality the vacuum vessel was more important for stabilisation than the coil cases, even though the latter were closer to the plasma. This is consistent with a theory of wall effects [27,28] which indicates that the poloidal extent of the piece of conducting structure can be of great importance to its effectiveness in wall stabilisation, even more important than proximity. A close "wall" with significant poloidal gaps is only as effective as a continuous wall that is farther away. The effective equivalent continuous wall representing the effect of the coil cases in MAST is likely farther than the actual vacuum vessel.

Now we turn our attention back to the projected equilibria for the MAST-U device. Figures 9 and 10 show the structure of the perturbation for an ideal unstable mode in the k25 MAST-U equilibrium that has been scaled to higher pressure above the no-wall limit. The perturbations in Fig. 9 are made by scaling the largest δB normal value to 0.375 m of normal displacement from the last closed flux surface. Two toroidal

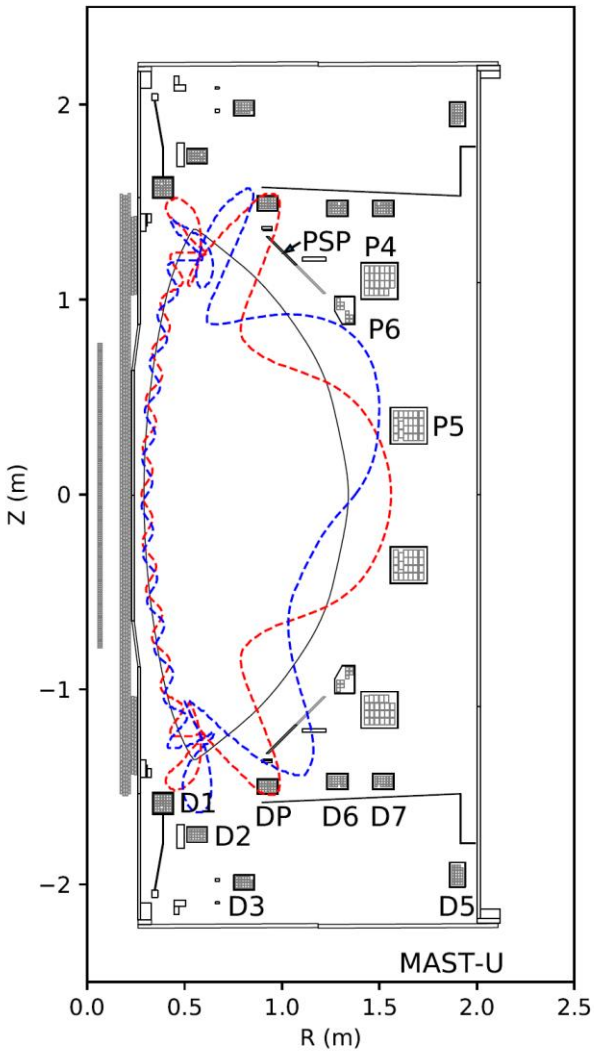

Figure 9. Exaggerated view of the perturbation, for an ideal unstable mode for MAST-U projected equilibrium k25 at β_N = 4.5 at zero (red) and ninety (blue) degrees toroidal.

cross sections of the 3D perturbation in Fig. 10 are shown in Fig. 9.

Although this perturbation is visually similar to what was previously found in the MAST case, there are some important differences. First, there is somewhat less of a ballooning shape on the outboard midplane. Second, there is significant mode perturbation in the region of the new MAST-U passive stabilisation plates, which can be seen in Fig. 9. This means that the global mode at high beta should couple well to the new conducting structure in MAST-U. Indeed, in Fig. 8, significant eddy currents are clearly visible in the upper and lower divertor structures. Though still not poloidally continuous, the divertor structures provide a larger poloidal coverage, and in an important region where the instability eigenmode

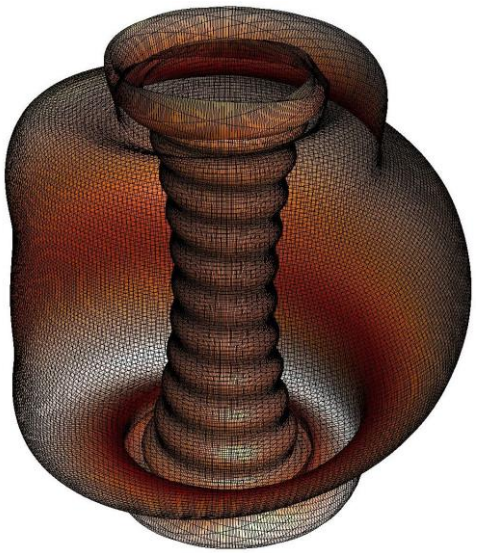

Figure 10. Exaggerated computed mode eigenfunction of the n = 1 resistive wall mode, using MAST-U projected equilibrium k25 at β_N = 4.5.

amplitude is large at high β_N,, thus acting more effectively at wall stabilisation than the coil cases alone in MAST.

When the β_N scan is performed for the k25 projected equilibrium in VALEN with the MAST-U conducting structure and realistic element resistivities, the no-wall limit, which is where the growth rate of the ideal mode starts in Fig. 12a, is found to be β_N = 3.91, which is close to the DCON value of 3.94. The transition from the resistive to ideal branches of the calculated growth rate can be seen in Fig. 12b, which shows the growth rate vs. a log scale of $C_\beta = (\beta_N - \beta_N^{no\text{-}wall})/(\beta_N^{with\text{-}wall} - \beta_N^{no\text{-}wall})$. Also included in the figures, in blue, is the growth rate with the conducting structure modelled as a super-conducting material, which indicated where the with-wall limit is located, at β_N = 5.95 (above which the mode would grow even with a super-conducting wall present). The gap between the no-wall limit and the with-wall limit, enabled by the increased wall stabilisation due to the stainless steel baffle structure, is apparent. This can also be seen, visually, by the thickness of the arrows of eddy current in the MAST-U structure, which are proportional to the amount of current flowing in a given element, in Fig. 9. The exact pattern of the eddy currents in the passive stabilisation plates may not be quite correct at the moment, due to the present simplification of the plates as fully toroidally continuous rather than only connected on their bottom halves. However, it is still clear that current in these plates is considerably closer to the plasma than any current was in MAST, and will improve the wall stabilisation of the plasma.

This analysis, and similar ones for the other equilibria, was the source of the with-wall limits for MAST-U indicated on Fig.

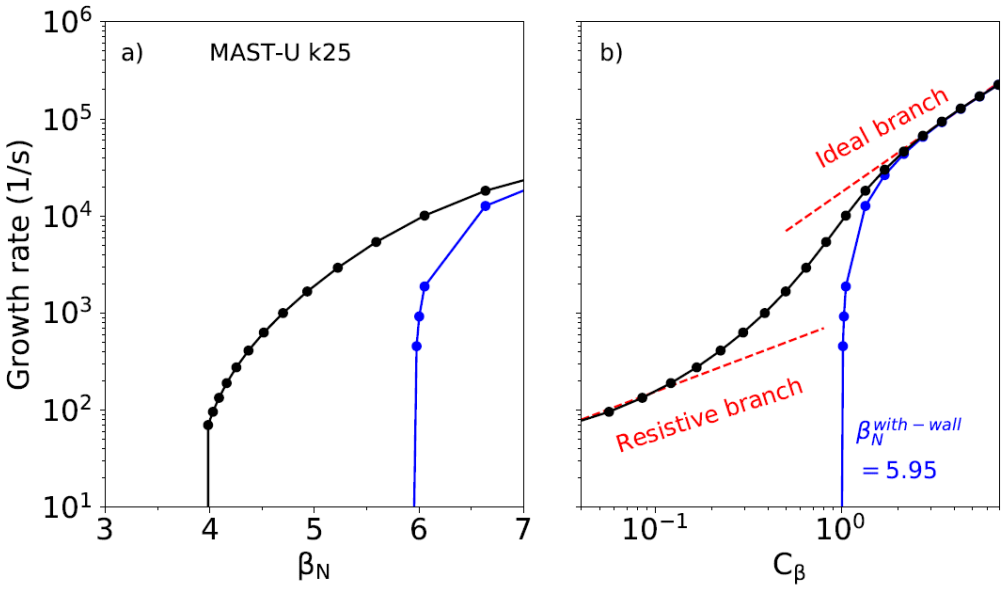

Figure 11. VALEN-calculated growth rates vs. (a) β_N, and (b) C_β, for MAST-U projected equilibrium k25. In black is the growth rate with the real MAST-U conducting structure, and in blue with a super-conducting wall.

5 with solid triangles. The trendline of β_N/l_i = 8.68, indicated in Fig. 5 with a dash-dot black line, is quite similar to the MARS-F with-wall limit, despite the differences in the way the wall was treated between the codes. The gaps between the no-wall and with-wall limits for the equilibria from DCON was 6.44-8.01, and from MARS-F was the slightly higher level, but similar span of 7.13-8.68. The increased operating space between the no-wall and with-wall beta limits should enable high beta wall-stabilised operation in MAST-U with a rotating plasma (when the plasma rotation frequency with respect to the conducting wall is faster than the inverse of the wall eddy current decay time, the wall acts like a superconductor). By the present ideal stability analysis, resistive wall modes should be unstable in that operating gap, however various other methods of passive and active stabilisation of the RWM have been demonstrated (e.g. kinetic stabilisation effects) which allow stable tokamak plasmas operation above the ideal no-wall stability limit [29,30].

5. Conclusions

The MAST-U device is an upgrade of the previous MAST spherical tokamak. One of the major differences, with respect to global stability of the plasma, between the devices is the presence of new conducting passive stabilisation plates in MAST-U. Through the study of four projected high beta equilibria we have shown that this new conducting structure enables a larger gap for potential high beta operation between the no-wall and with-wall limits. This gap was found to be roughly in the range of β_N between 4 and 5, with the MARS-F code given slightly higher values and DCON slightly lower. The MARS-F code finds an approximate no-wall limit of β_N/l_i = 7.13 and, with an axisymmetric wall, a with-wall limit of β_N/l_i = 8.53. The DCON code finds a no-wall limit around or slightly below β_N of 4 that increases with increasing l_i, at a rate of β_N/l_i = 6.44. There is a similarly sized gap between the limits from DCON and MARS-F, as the DCON with-wall limit, found with a wall with a poloidal gap, is β_N/l_i = 8.01. The VALEN code contains a three dimensional conducting structure model of MAST-U and indicates that the mode perturbation drives eddy current in the new divertor structures, which stabilises the ideal mode up to the with-wall limit of β_N/l_i = 8.68, similar to the MARS-F result, despite the differences in the wall model. Though they don't account for non-ideal stabilising effects of the RWM, these projected limits yield an analysis of the stable operational window in key parameters for MAST-U at high beta, indicating at what levels a plasma would be more susceptible to disruption.

Acknowledgements

The authors acknowledge the help of D. Battaglia, D. Brennan, L. Kogan, and J.-K. Park. This research was supported by the U.S. Department of Energy under contracts DE-SC0018623 (Columbia University), DE-AC02-09CH11466 (PPPL), and DE-FG02-95ER54309 and DE-FC02-04ER54698 (General Atomics). This work is also partly funded by the RCUK Energy Programme [grant number

EP/P012450/1]. To obtain further information on the data and models underlying this paper please contact PublicationsManager@ukaea.uk.

References

[1] Harrison J R *et al.* 2019 *Nucl. Fusion* **59** 112011
[2] Berkery J W *et al.* 2011 *Phys. Rev. Lett.* **106** 075004
[3] Bondeson A and Ward D 1994 *Phys. Rev. Lett.* **72** 2709
[4] Piovesan P *et al.* 2017 *Plasma Physics and Controlled Fusion* **59** 014027
[5] Berkery J W *et al.* 2017 *Physics of Plasmas* **24** 056103
[6] Sabbagh S A et al. 2018 IAEA Fusion Energy Conference (Gandhinagar, India) EX/P6-26
[7] Piccione A *et al.* 2020 *Nucl. Fusion* **60** 046033
[8] Hole M J *et al.* 2005 *Plasma Physics and Controlled Fusion* **47** 581
[9] Chapman I T *et al.* 2011 *Nucl. Fusion* **51** 073040
[10] Chapman I T *et al.*, 2011 *Plasma Physics and Controlled Fusion* **53** 065022
[11] Glasser A H 2016 *Physics of Plasmas* **23** 072505
[12] Liu Y Q *et al.* 2000 *Physics of Plasmas* **7** 3681
[13] Bialek J *et al.* 2001 *Physics of Plasmas* **8** 2170
[14] Cunningham G 2013 *Fusion Engineering and Design* **88** 3238
[15] Budny R V *et al.* 1992 *Nucl. Fusion* **32** 429
[16] Morris W *et al.* 2018 *IEEE Trans. on Plasma Sci.* **46** 1217
[17] Lutjens H *et al.* 1996 *Computer Physics Communications* **97** 219
[18] Berkery J W *et al.* 2015 *Nucl. Fusion* **55** 123007
[19] Liu Y Q *et al.* 2009 *Plasma Physics and Controlled Fusion* **51** 115005
[20] Ferron J R *et al.* 2005 *Physics of Plasmas* **12** 056126
[21] Crotinger J A *et al.* 1997 *LLNL Report* UCRL-ID-126284
[22] Chance M S 1997 *Physics of Plasmas* **4** 2161
[23] Battaglia D J *et al.* 2004 *Nucl. Fusion* **59** 126016
[24] Sabbagh S A *et al.* 2004 *Nucl. Fusion* **44** 560
[25] Morris W *et al.* 2018 *IEEE Trans. on Plasma Sci.* **46** 1217
[26] Buttery R J *et al.* 2004 *Nucl. Fusion* **44** 1027
[27] Ward D J 1996 *Physics of Plasmas* **3** 3653
[28] Fitzpatrick R 1997 *Physics of Plasmas* **4** 4043
[29] Berkery J W *et al.* 2010 *Physics of Plasmas* **17** 082504
[30] Sabbagh S A *et al.* 2006 *Phys. Rev. Lett.* **97** 045004